UAV-Based 5G Localization for Emergency Response Using Signals of Opportunity

Harish K. Dureppagari, Chiranjib Saha, Harpreet S. Dhillon, R. Michael Buehrer

Abstract—We exploit cellular signals of opportunity (SOPs) using 5G uplink (UL) sounding reference signals (SRS) to develop an indoor positioning system utilizing unmanned aerial vehicles (UAVs) for emergency services. To facilitate a rigorous evaluation, we introduce a novel 3rd Generation Partnership Project (3GPP) compliant system-level analytical framework that meticulously captures 5G physical layer aspects and largescale, and small-scale fading characteristics. This framework eliminates the need for exhaustive link-level simulations, making the validation process efficient. As an integral component of our proposed framework, we derive the Cramér-Rao lower bound (CRLB) for ranging and positioning errors in the presence of multipath propagation. This ensures an accurate performance evaluation, incorporating all 3GPP aspects. For the practical implementation of the proposed use case, we develop a lowcomplexity positioning algorithm: the iterative parallel projection method (IPPM). We conclude by providing insights from the evaluation and highlighting how the proposed framework aligns with the positioning requirements.

Index Terms—Cellular Signals of Opportunity, Public Safety, CIR-based CRLB, SRS, UTDOA.

I. INTRODUCTION

Indoor localization has gained significant attention recently due to its diverse applications [1], [2], including critical ones like locating distressed user equipment (UEs). However, due to poor signal quality, conventional Global Navigation Satellite Systems (GNSS) often prove unreliable in indoor settings. Additionally, relying on cellular base stations (BSs) for indoor positioning poses challenges, as it is uncertain to establish communication with an adequate number of BSs indoors. To address this issue, there has been a promising shift towards leveraging unmanned aerial vehicles (UAVs), also known as drones, as first responders [3], a concept often termed Drone as First Responder (DFR). This offers substantial potential for public safety applications like search and rescue operations and firefighting. Acknowledging the critical need for such applications, our paper focuses on a specific use case: a UAVbased indoor localization system designed to accurately locate UEs during emergency events.

A key question arises: "How to build infrastructure supporting a wide range of UEs and UAVs for the emerging public safety and emergency services?" To promote the development

H. K. Dureppagari, H. S. Dhillon, and R. M. Buehrer are with Wireless@VT, Department of ECE, Virginia Tech, Blacksburg, VA 24061, USA. Email: {harishkumard, hdhillon, rbuehrer}@vt.edu. C. Saha is with the Qualcomm Standards and Industry Organization, Qualcomm Technologies Inc., San Diego, CA 92121, USA. Email: csaha@qti.qualcomm.com. The support of the US NSF (Grants CNS-1923807 and CNS-2107276) and the US NIST (Grant CAN-70NANB22H070) is gratefully acknowledged.

of such services, the National Telecommunications and Information Administration (NTIA) established the First Responder Network Authority (FirstNet) in 2012, providing a nationwide broadband network with a special focus on public safety agencies and first responders. The Federal Communications Commission (FCC) designated LTE band 14 (700MHz) for FirstNet, paving the way for further advancements in public safety applications. Given the interest in location-based services for public safety, we introduce an emergency use case enabled by 5G, leveraging UAVs. Additionally, efforts are underway to expand the 5G C-band (3.7 to 4.2 GHz) to extend coverage, particularly in emergency scenarios. Target UEs, such as distressed UEs, receive emergency services, with 5G Next Generation Node B (gNB) mounted UAVs acting as first responders to locate them. An essential question emerges: can we enable this emergency use case using existing 5G reference signals used for communication purposes? To address this, we leverage the existing 5G uplink (UL) sounding reference signals (SRS), originally meant for channel sounding and UL frequency-selective scheduling [4], but adaptable for positioning purposes [5]. This concept is known as leveraging "Signal Reuse" or "Cellular Signals of Opportunity (SOPs)".

Recent efforts have explored UAV-based localization for emergency applications and navigation using cellular signals of opportunity (SOPs). These include a novel pseudomultilateration method for localization using continuous delay measurements from a single UAV [6], CRLB sensitivity analysis for precise indoor localization [7], and discussions on security and privacy aspects in drone-assisted public safety networks [8]. Leveraging cellular SOPs, studies assessed highaltitude aircraft navigation [9] and developed frameworks for sub-meter accuracy in UAV navigation [10]. In [11], non-terrestrial network (NTN)-based precise positioning is proposed as a potential alternative to GNSS systems. However, there has been limited emphasis on leveraging SOPs for positioning in emergency scenarios, and there is a lack of an accurate analytical and system-level framework to evaluate such applications.

Our contributions focus on leveraging SOPs for indoor emergency localization employing UAVs. We present a 3GPP-compliant analytical framework for evaluating such applications, incorporating physical layer aspects and large/small-scale fading parameters, thereby eliminating the need for extensive link-level simulations. Additionally, we adopt a low-complexity algorithm, the iterative parallel projection method (IPPM) [12], [13], by reformulating it for time-difference-of-arrival (TDOA) based positioning for real-time implementa-



Fig. 1: System model for the UAV-based emergency responding scenario, where the target UE requiring emergency service is being localized using 5G.

tion. Insights from our evaluation underscore the feasibility and accuracy of our proposed framework for realizing UAVbased emergency localization.

II. SYSTEM MODEL

The system model, depicted in Fig.1, features UAVs deployed outdoors to serve as anchors and UEs requiring emergency service indoors as target nodes. Our goal is to position anchors strategically to ensure each target node can communicate effectively with a sufficient number of anchors for accurate localization. To evaluate positioning performance, we adopt the dual stripe model [14], commonly used for analyzing cellular networks, especially in high-frequency and millimeter-wave (mmWave) communications scenarios. This model divides the environment into line-of-sight (LOS) and non-LOS (NLOS) regions, or "stripes,". LOS or NLOS stripe selection depends on the scenario, with LOS applied when both anchor and target UE are within the same building and NLOS otherwise. As our use case involves outdoor UAV deployment and indoor target UEs (excluding those on the roof), the NLOS stripe is predominantly used, while LOS propagation is assumed for rooftop UEs, detailed in Section V. The building model, as illustrated in Fig. 2, provides an example of how the evaluation model appears. In this model, each apartment, measuring 10m×10m, is separated by wall stripes. Target UEs (black squares) are uniformly distributed inside the apartments, while anchors (red diamonds) are placed outside. To account for the signal-to-noise ratio (SNR) between target UE and anchor links, large-scale parameters are incorporated [14]. For the anchor-to-target UE channel, we integrate clustered-delay-line (CDL) channel models [15], CDL-A for NLOS scenarios, and CDL-D for LOS scenarios.

It is important to understand the localization process presented in Fig.1. Initially, target UEs connect to a serving gNB (e.g., Anchor UAV1). Uplink TDOA (UTDOA) positioning begins with the UE requesting its position from the Location

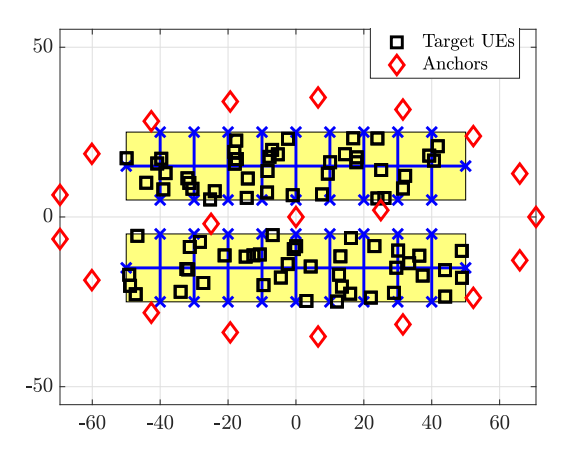


Fig. 2: Top view of an apartment unit illustrating UAVs/anchors being deployed outside the building and target UEs residing inside or on the rooftop of the building.

Management Function (LMF). The LMF then sends a positioning information request via the New Radio Positioning Protocol Annex (NRPPa) to the serving gNB. Next, the serving gNB determines the UL SRS configuration and initiates SRS transmission from the UE. NRPPa subsequently sends a measurement request to both the serving gNB and neighboring gNBs for UL time-of-arrival (TOA) measurements. These measurements are relayed to the LMF via NRPPa, enabling the LMF to calculate the precise location of the UE. For a more detailed procedure, readers are directed to [16].

III. PEB ANALYSIS

In this section, we present the CRLB of ranging and positioning for the 5G UL SRS transmission and reception, which is the main technical contribution of the paper. We will first derive the CRLB of TOA (or range) between anchors and one target UE, without loss of generality. Then we will derive the CRLB of the position estimate of the target UEs using TDOAbased localization. It is important to distinguish our approach from CRLB-based analyses in existing literature [17], [18]. In our scenario, the channels between the UAVs and target UEs are predominantly NLOS. While a closed-form expression of the CRLB of TOA exists for LOS channels [17], deriving the CRLB for NLOS channels is not straightforward. The standard method involves incorporating a gamma-distributed NLOS bias [18], but it lacks a clear connection to specific radio propagation conditions and the physical layer structure of the transmitted signal. It makes this method not suitable for scenarios where the large-scale and small-scale fading components are considered, along with the SRS signal generation and configuration aspects. As specified in [19], the SRS signal is generated using the Zadoff-Chu sequence as a base sequence, with the following representation:

$$\begin{split} r_{u,v}^{\alpha,\delta}(n) &= e^{j\alpha n} \bar{r}_{u,v}(n), \quad 0 \le n \le M_{ZC}, \\ \bar{r}_{u,v}(n) &= x_q \left(n \bmod N_{ZC} \right), \\ x_q(m) &= e^{-j\frac{\pi q m (m+1)}{N_{ZC}}}, \end{split} \tag{1}$$

where α defines the cyclic shift, δ denotes the comb structure, $\bar{r}_{u,v}(n)$ represents the base sequence, $u \in \{0,1,\dots,29\}$ denotes the group number, $v \in \{0,1\}$ signifies the base sequence number within the group, M_{ZC} indicates the length of the sequence, $q = \lfloor \bar{q} + \frac{1}{2} \rfloor + v.(-1)^{\lfloor 2\bar{q} \rfloor}$, $\bar{q} = N_{ZC}.\frac{u+1}{31}$, and N_{ZC} denotes the largest prime number such that $N_{ZC} < M_{ZC}$.

We denote $\mathcal{N}_b = \{1,2,\ldots,B\}$ be a set of anchor nodes that are assigned to the target UE for SRS reception. We call an SRS occasion the time interval (e.g. one slot) in which a set of anchors \mathcal{N}_b receive all SRSs from one target UE and each anchor coherently combines the associated N_{srs} SRS symbols. Within one SRS occasion, the time domain received signal can be represented in matrix form as

$$\mathbf{r}^k = \mathbf{F}^H \mathbf{X}^k \mathbf{\Gamma} \mathbf{F}_L \mathbf{h}^k + \mathbf{v}^k, \quad k = 0, \cdots, N_{srs} - 1,$$
 (2)

where k represents the OFDM symbol in an SRS occasion, \mathbf{r}^k denotes the time domain received SRS signal of length N, $\mathbf{v}^k \sim \mathcal{CN}(\mathbf{0}, \sigma^2\mathbf{I})$ represents additive-white-Gaussiannoise (AWGN), \mathbf{X}^k is the transmitted SRS in UL, $\mathbf{h}^k = \begin{bmatrix} h_0^k \cdots h_{L-1}^k \end{bmatrix}^T$ is the observed channel impulse response (CIR) between anchor and target UE, \mathbf{F}_L is a Discrete Fourier Transform (DFT) matrix of size $N \times L$, while \mathbf{F}^H is an inverse DFT (IDFT) matrix of size $N \times N$. Note that each delay tap of \mathbf{h}^k translates to a phase ramp in the frequency domain which is captured in

$$\Gamma = \operatorname{diag}\left(e^{-j2\pi\Delta f \tau_d(-\frac{N}{2})} \dots e^{-j2\pi\Delta f \tau_d(\frac{N}{2}-1)}\right).$$

For the whole SRS occasion, we can expand the matrix form in Equation (2) to jointly represent all the SRS symbols to be combined coherently as

$$\mathbb{R} = \mathbb{F}^H \mathbb{XGF}_L \mathbb{H} + \mathbb{V}, \tag{3}$$

where

$$\mathbb{R} = egin{bmatrix} m{r}^0 \ dots \ m{r}^{N_{srs}-1} \end{bmatrix}, \mathbb{H} = egin{bmatrix} m{h}^0 \ dots \ m{h}^{N_{srs}-1} \end{bmatrix}, \mathbb{V} = egin{bmatrix} m{v}^0 \ dots \ m{v}^{N_{srs}-1} \end{bmatrix}.$$
 $\mathbb{X} = \mathcal{B}\mathcal{D}m{X}^0 \cdots m{X}^{N_{srs}-1} \end{pmatrix}, \mathbb{G} = \mathcal{B}\mathcal{D}m{\Gamma} \cdots m{\Gamma} \end{pmatrix},$
 $\mathbb{F} = \mathcal{B}\mathcal{D}m{F} \cdots m{F} \end{pmatrix}, \mathbb{F}_L = \mathcal{B}\mathcal{D}m{F}_L \cdots m{F}_L \end{pmatrix},$

where
$$\mathcal{BD}(A^0\cdots A^{n-1})=egin{bmatrix}A^0&\cdots&\mathbf{0}\ dots&\ddots&dots\ \mathbf{0}&\cdots&A^{n-1}\end{bmatrix}$$
 . We now present the CPLR of TOA estimation A

We now present the CRLB of TOA estimation between the target UE and anchor as follows.

Theorem 1 (CRLB of TOA for one SRS Occasion). The variance of the TOA estimate between the target UE and anchor for one SRS occasion can be upper-bounded as:

$$var(\hat{\tau}_d) \ge \mathbb{I}_{e,\theta_{\hat{\tau}}}^{-1},$$
 (4)

where vector parameter $\boldsymbol{\theta}_{\tau}$ comprises τ_d and \mathbb{H} to facilitate the joint estimation of TOA and channel state information (CSI) and $\mathbb{I}_{e,\theta_{\tau}}$ is the effective Fisher information matrix (EFIM) representing TOA information. Denoting the TOA

estimate as $\hat{\tau}_d$, we can derive EFIM and subsequently the CRLB for the variance of $\hat{\tau}_d$ as

$$var(\hat{\tau}_{d}) \geq \mathbb{I}_{e,\theta_{\hat{\tau}}}^{-1},$$

$$\mathbb{I}_{e,\theta_{\hat{\tau}}} = \sum_{k=1}^{N_{srs}-1} \frac{2}{\sigma^{2}} \boldsymbol{h}^{kH} \boldsymbol{F}_{L}^{H} \boldsymbol{X}^{kH} \boldsymbol{D} \boldsymbol{\Xi}_{k} \boldsymbol{D} \boldsymbol{X}^{k} \boldsymbol{F}_{L} \boldsymbol{h}^{k}, \quad (5)$$

$$\boldsymbol{\Xi}_{k} = \left(\boldsymbol{I} - \boldsymbol{X}^{k} \boldsymbol{F}_{L} (\boldsymbol{F}_{L}^{H} \boldsymbol{X}^{kH} \boldsymbol{X} \boldsymbol{F}_{L})^{-1} \boldsymbol{F}_{L}^{H} \boldsymbol{X}^{kH} \right),$$

where $\frac{2}{\sigma^2}$ denotes the variance of noise samples and $D = \operatorname{diag}\left(2\pi\Delta f \tau_d(-\frac{N}{2}), \ldots, 2\pi\Delta f \tau_d(\frac{N}{2}-1)\right)$.

Note that the expression in (5) represents a generalized version of the derivation detailed in [20].

Having obtained the CRLB for the variance of the TOA error, and denoting FIM for the measurements between anchor b and the target UE by $I_{e,\theta^b_{\hat{\tau}}}$, we proceed to calculate the resultant FIM for TOA measurements from the set of anchors \mathcal{N}_b assigned to target UE as follows

$$\boldsymbol{I}_{\theta_{\hat{\tau}}} = \begin{bmatrix} \boldsymbol{I}_{e,\theta_{\hat{\tau}}^{1}} & \cdots & 0 \\ \vdots & \ddots & \vdots \\ 0 & \cdots & \boldsymbol{I}_{e,\theta_{\hat{\tau}}^{B}} \end{bmatrix}$$
(6)

Assuming anchor b=1 serves as a reference anchor, the TDOA measurements are obtained as

$$\tilde{\tau}_{d,b} = \hat{\tau}_{d,b} - \hat{\tau}_{d,1}, \quad \forall b \in \mathcal{N}_b \setminus 1.$$
 (7)

Denoting the vector parameter for TDOA estimation as $\theta_{\tilde{\tau}}$, the FIM for TDOA measurements derived from TOA measurements is expressed as

$$\boldsymbol{I}_{\theta_{\hat{\tau}}} = \left(\boldsymbol{J}_{\hat{\tau} \to \hat{\tau}} \boldsymbol{I}_{\theta_{\hat{\tau}}}^{-1} \boldsymbol{J}_{\hat{\tau} \to \hat{\tau}}^{T}\right)^{-1}, \tag{8}$$

where
$$J_{\hat{\tau} \to \tilde{\tau}}$$
 is defined as $J_{\hat{\tau} \to \tilde{\tau}} = \begin{bmatrix} -1 & 1 & \cdots & 0 \\ \vdots & \vdots & \ddots & \vdots \\ -1 & 0 & \cdots & 1 \end{bmatrix}$.

After obtaining the FIM for TDÖA, assuming 3D position estimation, we first define a position parameter $\boldsymbol{\theta}_p = [x, y, z]^T$, comprising the coordinates of the target UE. Additionally, we denote the coordinates of anchor b by $\mathbf{p}_b = [x_b, y_b, z_b]^T$, and represent the true range between anchor b and target UE as $d_b = ||\boldsymbol{\theta}_p - \mathbf{p}_b||$. Then, the FIM for $\boldsymbol{\theta}_p$, denoted by $I_{\tilde{\theta}_p}$, can be obtained as

$$\boldsymbol{I}_{\tilde{\theta}_{p}} = \boldsymbol{J}_{\tilde{\tau} \to \theta} \boldsymbol{I}_{\theta_{\tilde{\tau}}} \boldsymbol{J}_{\tilde{\tau} \to \theta}^{T}, \tag{9}$$

where $J_{\tilde{\tau}\to\theta}$ is the Jacobian transformation from TDOA measurements to the position parameter, and it is defined as

$$\boldsymbol{J}_{\tilde{\tau} \to \theta} = \begin{bmatrix} J_2 \\ J_3 \\ \vdots \\ J_B \end{bmatrix}^T, \text{ with } J_b = \begin{bmatrix} \frac{x - x_b}{d_b} - \frac{x - x_1}{d_1} \\ \frac{y - y_b}{d_b} - \frac{y - y_1}{d_1} \\ \frac{z - z_b}{d_b} - \frac{z - z_1}{d_1} \end{bmatrix}^T, \ \forall b \in \mathcal{N}_b \backslash 1.$$

The variance of the position estimate, also known as position error bound (PEB) is then given by

$$\operatorname{var}(\boldsymbol{\theta}_p) \ge \operatorname{trace}(\boldsymbol{I}_{\tilde{\boldsymbol{\theta}}_p}^{-1}).$$
 (10)

Algorithm 1: IPPM for TDOA-Based Localization

Data: Initial estimate $\hat{\theta}^0$, Convergence threshold ϵ , Maximum requisite consecutive iterations l **Result:** Final estimate $\hat{\theta}$ $\mathbf{R}^{0} \leftarrow \frac{1}{B-1} \sum_{b=2}^{B} \left(\hat{r}_{b} - \left(||\hat{\theta}^{0} - A_{b}|| - ||\hat{\theta}^{0} - A_{1}|| \right) \right)^{2}$ while True do $\hat{\theta}^k \leftarrow$ $\frac{1}{B-1} \sum_{b=2}^{B} \left(A_b + \left(\hat{r}_b + ||\hat{\theta}^{k-1} - A_1|| \right) \frac{\hat{\theta}^{k-1} - A_b}{||\hat{\theta}^{k-1} - A_b||} \right)^{2}$ $\mathbf{R}^{k} \leftarrow \frac{1}{B-1} \sum_{b=2}^{B} \left(\hat{r}_{b} - \left(||\hat{\theta}^{k} - A_{b}|| - ||\hat{\theta}^{k} - A_{1}|| \right) \right)$ if $|\mathbf{R}^k - \mathbf{R}^{k-1}| < \epsilon$ then $w \leftarrow w + 1$ if $w \ge l$ then $\hat{\theta} \leftarrow \hat{\theta}^k$ break else $\lfloor w \leftarrow 0$ $k \leftarrow k + 1$

IV. LOW COMPLEXITY POSITIONING ALGORITHM

In this section, we focus on a low-complexity localization algorithm known in the literature as IPPM. We consider a network of B anchors assigned to a target UE to obtain range measurements. The IPPM introduced in [12], is designed for TOA-based localization. As given in [12], the position estimate at the k-th iteration, denoted by $\hat{\theta}^k$, is updated using the position estimate from the previous iteration, denoted by $\hat{\theta}^{k-1}$. The recursive loop terminates when the difference between consecutive TOA residual error values is less than a specified threshold, denoted by ϵ , which is typically set to a very small value (e.g., on the order of 0.001).

To adapt IPPM for TDOA-based localization, Algorithm 1 outlines the necessary reformulations. This involves changing the TOA residual error to the TDOA residual error (see Step (2)). Assuming anchor b = 1 functions as a reference anchor, the weights for the parallel projections of $\hat{\theta}^{k-1}$ are determined by TDOA measurements and estimated range measurements for the reference anchor. Similar to IPPM for TOA-based localization, Algorithm 1 terminates its recursive loop when the difference between consecutive TDOA residual error values falls below ϵ . Importantly, IPPM offers low computational complexity compared to conventional algorithms like non-linear least squares (NLS) and recursive weighted least squares (RWLS) [21] because it avoids matrix inversions. Remarkably, IPPM achieves performance comparable to NLS while offering this computational advantage which we discuss in the next section.

V. RESULTS AND DISCUSSIONS

In this section, we embark on a comprehensive evaluation of positioning performance. To provide context, we categorize target UEs into two distinct types in our evaluation: outdoor

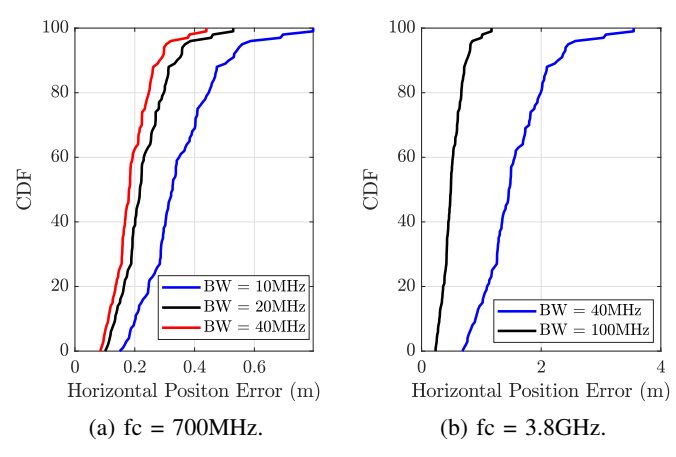


Fig. 3: Indoor UE Scenario: CDF of Horizontal Positioning Error.

target UEs and indoor target UEs. Outdoor UEs are the UEs positioned on the roof with an open top, for which we assume LOS links with anchors, characterized by an absence of wall crossings and penetration losses. Conversely, indoor UEs are always assumed to be in NLOS with anchors, involving wall crossings, and penetration losses that are modeled using the dual stripe path loss model [14]. The intricacies of shadow fading are also considered based on LOS/NLOS links. To incorporate small-scale fading, we opt for the CDL-D channel model for outdoor UEs and CDL-A for indoor UEs. Furthermore, our analysis considering fc = 2GHz with 20MHz illustrates that CDL-A results in high TOA error (~38ns at SNR = 5dB), compared to the TOA error (\sim 15ns at SNR = 5dB) observed in the CDL-D channel model. Regarding the positioning method, we use UTDOA-based localization, as it is commonly preferred in the field due to its advantages in not requiring strict synchronization between anchors and target UEs and exhibiting increased robustness against NLOS effects.

Before delving into the evaluation of positioning error, it is crucial to emphasize the assumptions made in the CRLB analysis presented in Section III. Specifically, we assumed the following: 1) Perfect synchronization among anchors and between anchors and UEs is assumed. 2) SRS intended for communication is typically transmitted over narrowband, which is hopped over time to collect wideband SRS. This practice is necessitated by the limited transmit power at the UE, and more often than not, the UE is scheduled over a narrowband. 3) As narrowband SRSs are collected over time, we assume channel coherence throughout SRS collection while estimating TOA. Having said that, as a natural extension of this effort, our future work includes incorporating noncoherent combining strategies for multiple SRS transmissions, especially when the combining interval extends beyond the channel coherence time.

We now delve into the assessment of positioning performance. For our investigation, we deploy a network consisting of 20 anchors and 100 target UEs. The indoor scenario involves the uniform distribution of target UEs within the

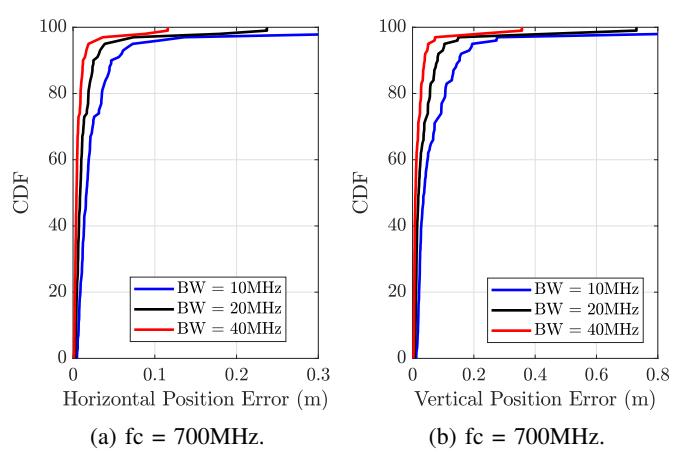


Fig. 4: Outdoor UE Scenario: CDF of Horizontal and Vertical Positioning Error.

TADI	T	т	T 1	. •	Parameters
IAKI	н	ι.	HVallia	าบาก	Parameters

Parameter	Simulation Assumptions			
Carrier frequency (fc)	700MHz (FirstNet Band 14); 3.8GHz (5G			
	C-Band)			
Subcarrier spacing	15KHz; 30KHz			
SRS bandwidth	10, 20, and 40MHz (fc = 700MHz), 40			
	and $100MHz$ (fc = $3.8GHz$)			
SRS structure and re-	Comb-4 and 4 SRS symbols without in-			
source allocation	terference			
Large Scale Fading	Dual-stripe model			
Shadow Fading	Log-Normal distribution (standard devia-			
	tion: 4dB/7dB for LOS/NLOS)			
Small Scale Fading	CDL-D (for LOS/outdoor UEs); CDL-A			
	(for NLOS/indoor UEs)			
Maximum transmit power	23dBm			
Thermal noise power	-174dBm/Hz			
Anchor assignment	4 anchors based on SNR			
Key performance indica-	TOA error, and Horizontal and Vertical			
tors	positioning error			

building, while the outdoor scenario assumes UEs are distributed on the roof, as illustrated in Fig. 2. Additional evaluation assumptions are as given in Table I. To create a simulated environment, we position the anchors on an outer ellipse surrounding the building as depicted in Fig. 2. After assigning anchors to each target UE based on SNR, we conduct CRLB analysis, as discussed in Section III, to compute TOA error values for each UE for each assigned anchor, as given in Equation (5). Subsequently, we calculate position error for each UE using TDOA-based localization, as given in Equation (10).

Fig. 3a and. 3b present the CDF of horizontal positioning error obtained using CRLB (see Section III) for indoor target UEs for fc 700MHz and 3.8GHz respectively. Increased bandwidth contributes to enhanced positioning accuracy. The positioning error results demonstrate the feasibility of meeting stringent positioning requirements for public safety at 700MHz and 3.8GHz (with 100MHz bandwidth), as detailed in [22]. These results emphasize the critical significance of the 700MHz band and the capabilities of 3.8GHz in the context of public safety applications. Moreover, our preliminary results,

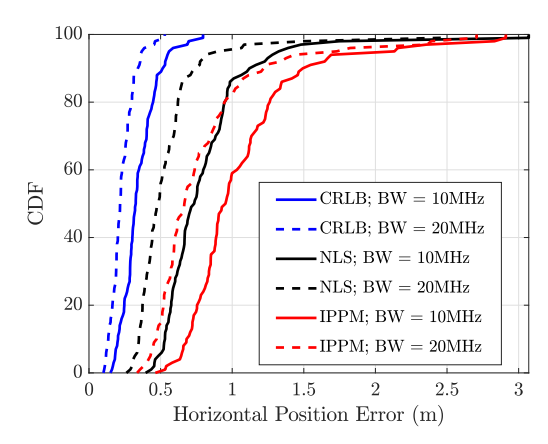


Fig. 5: Comparing CRLB, IPPM, and NLS for 700MHz with bandwidth 10 and 20MHz considering indoor target UEs.

indicating z-axis errors on the order of tens of meters, suggest that considering z-axis resolution for indoor UEs may not be meaningful. This is attributed to the penalties imposed by the NLOS channel model and substantial indoor penetration losses. Note that, z-axis accuracy is expected to be improved by utilizing more relevant models for large-scale and small-scale parameters designed for specific use cases.

We now proceed to assess the positioning performance of outdoor UEs, building upon the previously outlined simulation assumptions. In this evaluation, the target UEs are located on the roof and anchors are positioned not only around the building but also in the zenith. As outdoor UEs predominantly experience LOS propagation, we omit outdoor-to-indoor penetration losses. Employing the CDL-D channel model for small-scale fading, Fig.4a and Fig.4b present the CDF of horizontal and vertical positioning error for outdoor target UEs at fc = 700MHz, respectively. Due to reduced losses and subsequent minimized ranging errors, the results demonstrate compliance with positioning requirements for both horizontal and vertical positioning requirements. Furthermore, our findings suggest the feasibility of meeting positioning requirements, even in the 3.8 GHz band, particularly with a 100 MHz bandwidth.

In our final assessment, we focus on the performance evaluation of the low-complexity algorithm detailed in Section IV specifically for indoor UEs. This evaluation focuses on the 700MHz band with 10 and 20MHz bandwidths, employing the CDL-A channel model. The large-scale parameters and SRS configuration align with the previously described setup. To evaluate the efficacy of IPPM, we conduct a comparative analysis with the widely recognized NLS algorithm, as outlined in [21]. Fig.5 presents a comparative analysis, showcasing that although IPPM does not achieve CRLB, it demonstrates comparable performance to NLS with a significant advantage in terms of computational complexity.

VI. CONCLUDING REMARKS

In this paper, we have presented a UAV-based indoor localization system designed for emergency response, leveraging cellular SOPs within the realm of 5G. To provide a detailed understanding of how our proposed use case integrates into the 5G landscape, we introduced a novel analytical framework for a comprehensive system-level analysis. Our framework includes rigorous CRLB analysis, integrating physical layer, large-scale, and small-scale fading models recommended by 3GPP. Notably, our framework accurately abstracts systemlevel aspects, eliminating the need for time-consuming linklevel simulations. Our evaluation results provide several important insights including the critical importance of the 700MHz band for public safety applications, the capabilities of the 3.8GHz band, especially with a 100MHz bandwidth, and the nuanced impact of the physical layer, large-scale, and small-scale parameters. Furthermore, we proposed a lowcomplexity algorithm, demonstrating comparable performance to well-known methods such as NLS, while offering significant advantages in terms of computational complexity.

APPENDIX

A. Proof-sketch of Theorem 1

This section presents a proof sketch instead of a detailed proof due to space limitations. A comprehensive proof will be provided in the extended version of this paper. The following steps outline the derivation of the CRLB for TOA estimation across multiple SRS symbols.

- 1) Joint Likelihood Function. For the received signal model given in Equation (3), we can express the likelihood function as $p(\mathbb{R}|\tau_d,\mathbb{H}) = \prod_{k=1}^{N_{srs}-1} p(\mathbf{r}^k|\tau_d,\mathbf{h}^k)$, where $p(\mathbf{r}^k|\tau_d,\mathbf{h}^k)$ is the likelihood function of the signal received in k-th SRS OFDM symbol.
- 2) Define Resultant FIM. Formulate the FIM, denoted by $\mathbb{I}_{\theta_{\hat{\tau}}}$, for joint estimation of TOA and CSI $\theta_{\hat{\tau}} = [\tau_d \, Re(\mathbb{H}^T) \, Im(\mathbb{H}^T)]^T$ as

$$\sum_{k=0}^{N_{prs}-1} E\left(\left(\frac{\partial \log p(\mathbf{r}^k|\tau_d, \mathbf{h}^k)}{\partial \theta_{\hat{\tau}}}\right) \left(\frac{\partial \log p(\mathbf{r}^k|\tau_d, \mathbf{h}^k)}{\partial \theta_{\hat{\tau}}}\right)^T\right)$$
(11)

3) Calculate FIM Entries and EFIM. As the resultant FIM, shown in (11), is the summation of the FIM associated with individual SRS symbols, we compute the entries of FIM, denoted by $\boldsymbol{I}_{\theta_{\hat{\tau}}}$, for one SRS symbol. We then express $\boldsymbol{I}_{\theta_{\hat{\tau}}}$ in the form $\boldsymbol{I}_{\theta_{\hat{\tau}}} = \begin{bmatrix} A & B \\ B^H & C \end{bmatrix}$ and effective FIM (EFIM) for τ_d is calculated as [17] $\boldsymbol{I}_{e,\theta_{\hat{\tau}}} = (A - BC^{-1}B^H)$. Obtained EFIM is given as

$$I_{e,\theta_{\hat{\tau}}} = \frac{2}{\sigma^2} h^H F_L^H X^H D \Xi D X F_L h, \qquad (12)$$

$$\Xi = \left(I - X F_L (F_L^H X^H X F_L)^{-1} F_L^H X^H \right).$$

4) Obtain Resultant EFIM. Denoting the EFIM $I_{e,\theta\hat{\tau}}$ as $I_{e,\theta\hat{\tau}}^k$, substitute $I_{e,\theta\hat{\tau}}^k$ into Equation (11), where index k is to account for multiple SRS symbol transmissions. The final expression as given in the Equation (5) can be obtained by algebraic manipulation.

REFERENCES

- [1] H. Obeidat, W. Shuaieb, O. Obeidat, and R. Abd-Alhameed, "A Review of Indoor Localization Techniques and Wireless Technologies," *Wireless Pers. Commun.*, vol. 119, 07 2021.
- [2] F. Zafari, A. Gkelias, and K. K. Leung, "A Survey of Indoor Localization Systems and Technologies," *IEEE Commun. Surv. Tutor.*, vol. 21, no. 3, pp. 2568–2599, 2019.
- [3] M. Mozaffari, W. Saad, M. Bennis, Y.-H. Nam, and M. Debbah, "A tutorial on uavs for wireless networks: Applications, challenges, and open problems," *IEEE Commun. Surv. Tutor.*, vol. 21, no. 3, pp. 2334– 2360, 2019.
- [4] X. Lin, J. Li, R. Baldemair, J.-F. T. Cheng, S. Parkvall, D. C. Larsson, H. Koorapaty, M. Frenne, S. Falahati, A. Grovlen, and K. Werner, "5G New Radio: Unveiling the Essentials of the Next Generation Wireless Access Technology," *IEEE Commun. Stand. Mag.*, vol. 3, no. 3, pp. 30–37, 2019.
- [5] H.-S. Cha, G. Lee, A. Ghosh, M. Baker, S. Kelley, and J. Hofmann, "5G NR Positioning Enhancements in 3GPP Release-18," 2024, Available online: arxiv.org/abs/2401.17594.
- [6] V. S. A. Albanese and X. Costa-Pérez, "First responders got wings: UAVs to the rescue of localization operations in beyond 5G systems," *IEEE Commun. Mag.*, vol. 59, no. 11, pp. 28 – 34, Nov. 2021.
- [7] H. K. Dureppagari, D.-R. Emenonye, H. S. Dhillon, and R. M. Buehrer, "UAV-Aided Indoor Localization of Emergency Response Personnel," in 2023 IEEE/ION PLANS, 2023, pp. 1241–1249.
- [8] D. He, S. Chan, and M. Guizani, "Drone-assisted public safety networks: The security aspect," *IEEE Commun. Mag.*, vol. 55, no. 8, pp. 218–223, 2017.
- [9] Z. M. Kassas, J. Khalife, A. Abdallah, C. Lee, J. Jurado, S. Wachtel, J. Duede, Z. Hoeffner, T. Hulsey, R. Quirarte, and R. Tay, "Assessment of cellular signals of opportunity for high-altitude aircraft navigation," *IEEE Aerosp. Electron. Syst. Mag.*, vol. 37, no. 10, pp. 4–19, 2022.
- [10] J. Khalife and Z. M. Kassas, "On the achievability of submeter-accurate uav navigation with cellular signals exploiting loose network synchronization," *IEEE Trans. Aerosp. Electron. Syst.*, vol. 58, no. 5, pp. 4261–4278, 2022.
- [11] H. K. Dureppagari, C. Saha, H. S. Dhillon, and R. M. Buehrer, "NTN-Based 6G Localization: Vision, Role of LEOs, and Open Problems," *IEEE Wirel. Commun.*, vol. 30, no. 6, pp. 44–51, 2023.
- [12] T. Jia and R. M. Buehrer, "A Set-Theoretic Approach to Collaborative Position Location for Wireless Networks," *IEEE Trans. Mob. Comput.*, vol. 10, no. 9, pp. 1264–1275, 2011.
- [13] ——, "Collaborative Position Location for Wireless Networks Using Iterative Parallel Projection Method," in *IEEE GLOBECOM*, 2010, pp. 1_6
- [14] "Technical Specification Group Radio Access Network; Evolved Universal Terrestrial Radio Access (E-UTRA); Further advancements for E-UTRA physical layer aspects (Release 9)," 3GPP TR 36.814, version 9.2.0.
- [15] "5G; Study on channel model for frequencies from 0.5 to 100 GHz (Release 17)," 3GPP TR 38.901, version 17.0.0.
- [16] "Technical Specification Group Radio Access Network; NG Radio Access Network (NG-RAN); Stage 2 functional specification of User Equipment (UE) positioning in NG-RAN (Release 17)," 3GPP TS 38.305, version 17.6.0, Sep. 2023.
- [17] Y. Shen and M. Win, "Fundamental limits of wideband localization part I: A general framework," *IEEE Trans. Inf. Theory*, vol. 56, no. 10, pp. 4956 4980, Oct. 2010.
- [18] Y. Qi, H. Kobayashi, and H. Suda, "Analysis of wireless geolocation in a non-line-of-sight environment," *IEEE Trans. Wireless Commun.*, vol. 5, no. 3, pp. 672 – 681, Mar. 2006.
- [19] "Technical Specification Group Radio Access Network; NR; Physical channels and modulation (Release 18)," 3GPP TS 38.211, version 18.0.0, Sep. 2023.
- [20] D. Luan, "Fundamental Performance Limits on Time of Arrival Estimation Accuracy with 5G Radio Access (Degree project)," 2017, KTH Royal Institute of Technology Publications Database.
- [21] S. M. Kay, Fundamentals of Statistical Processing: Estimation Theory, Volume 1. Prentice-Hall, Inc, 1993.
- [22] "Technical Specification Group Radio Access Network; Study on scenarios and requirements of in-coverage, partial coverage, and out-of-coverage NR positioning use cases (Release 17)," 3GPP TR 38.845, version 17.0.0, Sep. 2021.